

Accelerating Vision Transformers Based on Heterogeneous Attention Patterns

Deli Yu* Teng Xi* Jianwei Li* Baopu Li† Gang Zhang
 Haocheng Feng Junyu Han Jingtuo Liu Errui Ding Jingdong Wang
 Department of Computer Vision Technology(VIS), Baidu Inc.

{yudeli, xiteng01, lijianwei04, baopuli, zhanggang03}@baidu.com
 {fenghaocheng, hanjunyu, liujingtuo, dingerrui, wangjingdong}@baidu.com

Abstract

Recently, Vision Transformers (ViTs) have attracted a lot of attention in the field of computer vision. Generally, the powerful representative capacity of ViTs mainly benefits from the self-attention mechanism, which has a high computation complexity. To accelerate ViTs, we propose an integrated compression pipeline based on observed heterogeneous attention patterns across layers. On one hand, different images share more similar attention patterns in early layers than later layers, indicating that the dynamic query-by-key self-attention matrix may be replaced with a static self-attention matrix in early layers. Then, we propose a dynamic-guided static self-attention (DGSSA) method where the matrix inherits self-attention information from the replaced dynamic self-attention to effectively improve the feature representation ability of ViTs. On the other hand, the attention maps have more low-rank patterns, which reflect token redundancy, in later layers than early layers. In a view of linear dimension reduction, we further propose a method of global aggregation pyramid (GLAD) to reduce the number of tokens in later layers of ViTs, such as DeiT. Experimentally, the integrated compression pipeline of DGSSA and GLAD can accelerate up to 121% run-time throughput compared with DeiT, which surpasses all SOTA approaches.

1. Introduction

Recently, Vision Transformers (ViTs) have shown their impressive capabilities in many computer vision tasks such as image classification [6, 11, 17, 17, 19, 20, 23, 30, 33, 41], object detection [4, 5, 13, 14, 46], semantic segmentation [36, 39, 42, 44] and so on. The impressive representative capacity of ViTs mainly comes from the self-attention (SA) mechanism of capturing the long range semantic dependencies,

which are difficult for previous convolution neural networks (CNNs). However, the quadratic calculation complexity of self-attention still limits its further applications, especially on resource-constrained scenarios.

To achieve efficient computation, the standard self-attention is modified with a new form of sparse versions [1, 2, 8, 22, 25, 26, 43]. Meanwhile, some efforts [27, 32] rethink the necessity of dynamic self-attention and replace it with a form of static self-attention (SSA) matrix, which is shared by all images. Thus, the repeated computation of dynamic self-attention matrix can be saved. Static form is more hardware-friendly than sparse form in run-time mode, due to no dependencies on specialized hard-and soft-ware framework. Since the complexity of self-attention is related to token numbers, another line prunes [28, 31, 40] or aggregates [10, 23, 35, 38] tokens, and can get a slimmed pyramid distribution of token numbers and largely increase run-time throughput too.

Some aforementioned works are motivated by the observed attention patterns of Transformers in NLP, but there are little related explorations for ViTs. Therefore, we make observations and find heterogeneous attention patterns in ViTs. As shown in Fig. 1, the attention maps of three different images chosen from ImageNet [16] have more similar patterns in early layers than later layers, while have more low-rank patterns in later layers than early layers for the well-known ViT model of DeiT-Small [33]. Obviously, low-rank patterns indicate the redundancy of tokens.

However, MLP-Mixer [32] assumes similar patterns in all the layers for their attention computation, which is obviously contradictory to our findings in Fig. 1. In addition, prior token pyramid methods [10, 23, 28, 31, 35, 38, 40] cannot accelerate the whole ViTs, because token redundancy is relatively low and token number is always kept nearly unchanged after compression in early layers, as Fig. 1(d) indicates.

Inspired by the observed heterogeneous attention patterns, we propose an integrated compression pipeline that exploits both similar patterns across images in early lay-

*Equal contribution.

†Corresponding author.

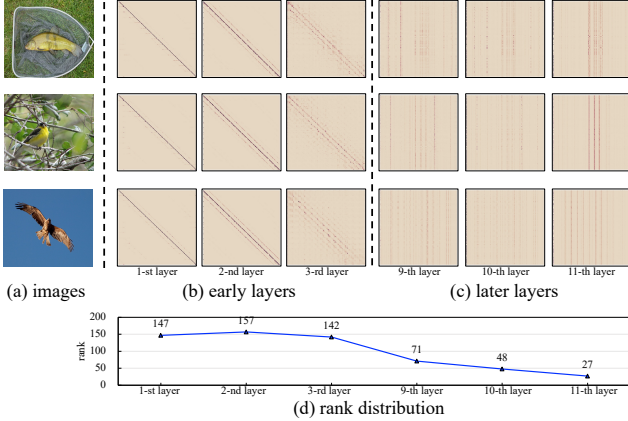


Figure 1. Inhomogeneous attention patterns across layers in ViTs. (a) are three samples. (b) and (c) are token-by-token attention maps of corresponding heads of (a) in early 1-th, 2-nd and 3-rd layer and later 9-th, 10-th and 11-th layer for Deit-Small, respectively. The row axis represents tokens, and the column axis represents the self-attention similarity coefficients by which the current token attends all tokens in these attention maps. (d) shows the rank distribution of the attention maps across these layers when eigenvalues are truncated at 99% accumulated energy .

ers and low-rank patterns in later layers to overcome the drawbacks of previous works and accelerate a whole ViT model. As shown in Fig. 2, this integrated model compression scheme includes two key parts, that is, dynamic-guided static self-attention (DGSSA) and Global Aggregation Pyramid (GLAD).

To boost the performance of static self-attention (SSA), we have SSA inherit some information from the dynamic SA rather than discarding it away, like [27, 32]. So DGSSA is first proposed to leverage the replaced dynamic attention to initialize the trainable attention matrices. Besides, motivated by the low-rank patterns, we propose a method of GLAD to reduce token numbers according to rank, which reflects the required minimum number of tokens to represent the attention map. GLAD can aggregate the full number of tokens into less number of tokens in a *global* scope by a linear projection. The contributions of this work can be summarized as follows:

- 1) A novel method of DGSSA for early layers to save computation is proposed. Differently, the static self-attention matrices are initialized with the self-attention information inherited from the dynamic self-attention.

- 2) We advance a new method of GLAD to reduce token numbers in later layers. Different from pruning-based methods and local aggregation methods, GLAD aggregates tokens globally by a linear projection, which can be more compatible to real spatial distribution of token redundancy.

- 3) Extensive experiments validate the effectiveness of DGSSA, GLAD and the integrated pipeline comprising the two methods. The integrated pipeline can accelerate up to about 121% run-time throughput of Deit.

2. Related Works

2.1. Efficient self-attention

To reduce computation and memory consumed by self-attention, its architecture is modified with a new more efficient form of sparse, low-rank and static versions.

Sparse self-attention is adopted by some works to handle long sequence. Parmar *et al.* [25] restricts the self-attention mechanism to attend local neighborhoods rather than all positions. Qiu *et al.* [26] uses block-wise sparse attention. Child *et al.* [9] uses sparse factorizations of the full attention matrix, and that sparse version makes attending at fixed intervals. Longformer [2] adopts not only that sparse pattern but also a few additional task-motivated global attention patterns. The Reformer [22] uses locality sensing hashing (LSH) to find and attend the nearest neighbors of the attention query. Routing Transformer [29] uses online k-means to learn dynamic sparse attention patterns, and thus avoids the computation of attending to the unrelated content. Beyond pure local attention, ETC [1] uses a global-local attention mechanism. BigBird [43] combines global-local attention and random sparse attention, and proves such kind of sparse attention is an universal approximator of sequence functions and Turing complete.

Low-rank self-attention is also explored to yield efficient self-attention, besides sparsity. Linformer [34] demonstrates that the self-attention mechanism can be approximated by a low-rank matrix. To encode fine-grained local information, Transformer-LS [45] integrated a novel low-rank projected long-range attention and a local window attention.

Static self-attention can accelerate the self-attention by using a static attention matrix shared by all images instead of calculating repeatedly attention matrix for each images. MLP-Mixer [32] proposes an architecture based exclusively on MLPs, two kinds of which mix the per-location features and spatial information, respectively. The latter mixing MLPs are analogical to trainable static attention matrices. Raganato *et al.* [27] replaces all but one attention head of each encoder layer with static non-trainable attention patterns that are solely based on position in NLP tasks. ConViT [15] introduces trainable gated combination of standard self-attention and positional self-attention, which is equivalent to a convolutional layer with inductive bias.

The proposed method is different from the above methods in two aspects. Firstly, our method only applies static attention for early layers instead of all layers. Secondly, our method initializes the static matrices under the guidance of dynamic self-attention.

2.2. Token Pyramid

ViTs can be accelerated by pruning or aggregating tokens. Since less tokens remain in the more later layers, there

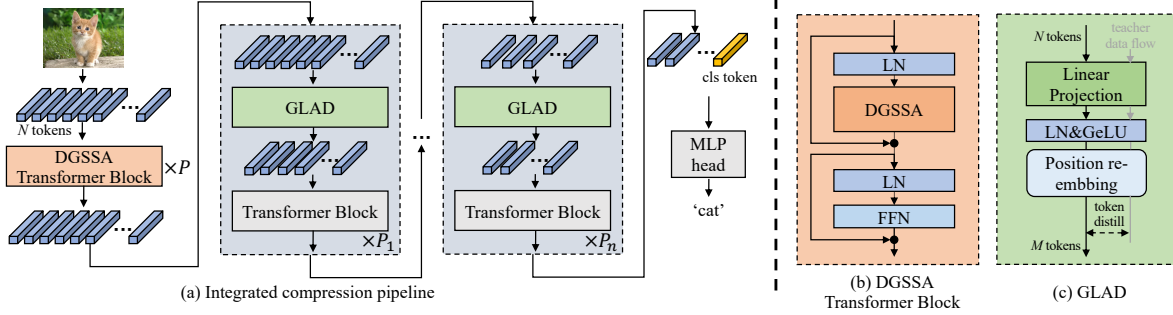


Figure 2. The integrated compression pipeline of dynamic-guided static self-attention (DGSSA) and global aggregation pyramid (GLAD). (a) is the integrated pipeline which replaces dynamic self-attention with DGSSA and keeps other modules unchanged in early P layers, and inserts GLAD to reduce the redundant tokens and get a pyramid structure of token numbers in later layers. (b) is the transformer block with DGSSA, and (c) illustrates GLAD.

is a structured or unstructured token pyramid.

Pruning-based methods. Patch Slimming [31] prunes useless patches in a top-down paradigm, where the effective patches are firstly identified in the last layer and then used to guide the patch selection of previous layers. DynamicViT [28] discards redundant tokens progressively and dynamically based on the importance score, which is provided by lightweight prediction module. Evo-ViT [40] updates the selected informative tokens and uninformative tokens with different computation paths, which is called slow-fast token evolution. ATS [18] samples informative tokens and discards uninformative tokens from token scoring distribution. TOME [3] prunes tokens by merging two tokens with high similarity after bipartite soft matching. TPS [37] first selects uninformative tokens, and then squeeze them informative tokens to reduce token numbers. However, pruning-based methods will drop spatial information of token sequences, and the lost information is never recovered in later stages.

Aggregation-based methods. Some works progressively shrink the pyramid of feature maps stage by stage. Then, the shrunk feature maps are flattened into smaller sequence of tokens back. Shrinking feature maps can preserve more spatial information than pruning-based methods. Swin [23] and Twins [10] concatenate 2×2 local neighboring tokens into one and extend feature dim C to $4C$. A following linear layer is applied on the $4C$ -dimensional concatenated features. CvT [38] uses down-sampling with fixed stride to get smaller spatial size of feature maps.

Unlike these local aggregation-based methods, the proposed GLAD makes global aggregation of tokens by a linear projection.

3. Methods

In this section, we first review the dynamic self-attention. Then, static self-attention and its dynamic-guided form are introduced to relieve computation of self-attention in early layers. Next, we introduce GLAD to reduce token numbers for later layers. Finally, we give an unified framework to

integrate both methods in a given ViT.

3.1. Review of Dynamic Self-Attention

Self-Attention (SA) is the key component of Transformers. SA aggregates the sequence features $X \in \mathbb{R}^{N \times d}$ by multiplying its value embeddings $XW_v \in \mathbb{R}^{N \times d}$ with self-attention matrix $A \in \mathbb{R}^{N \times N}$, where A is determined by the similarity of its query embeddings $XW_k \in \mathbb{R}^{N \times d}$ and its key embeddings $XW_q \in \mathbb{R}^{N \times d}$ using inner dots. The whole formulation of SA is as follows:

$$\begin{cases} A = \text{softmax}\left(\frac{XW_kW_q^T X^T}{\sqrt{d}}\right) \in \mathbb{R}^{N \times N} \\ \text{SA}(X) = AXW_k \in \mathbb{R}^{N \times d}, \end{cases} \quad (1)$$

where $W_k, W_q, W_v \in \mathbb{R}^{d \times d}$ are trainable matrices. The process of SA is conducted like Fig. 3(a). It is obvious that the calculation complexity of SA is quadratic to the token numbers N , and is unbearable when facing up high resolution of images with large N .

3.2. Dynamic-Guided Static Self-Attention

In this part, to relieve the computation of SA, we introduce the static self-attention (SSA) applied in the early layers of ViTs. Then, we discuss the drawbacks of two existing forms of SSA. Finally, a new type of SSA is proposed.

3.2.1 Static Self-Attention

We observe that the different images share similar self-attention matrix A in early layers of ViTs shown in Fig. 1 (b), despite the dynamic manner in nature. Assuming there is static self-attention matrix \hat{A} , which is an optimal estimation of A . We use it to replace A in Eq. 1, and obtain the static self-attention (SSA), as follows:

$$\text{SSA}(X) = \hat{A}XW_k \in \mathbb{R}^{N \times d}. \quad (2)$$

In this way, the calculation may be more efficient due to getting rid of the quadratic complexity of attention matrix A .

The characteristic of attention patterns makes this simplification plausible, and thus the application of efficient SSA may not cause much accuracy drop in early layers.

3.2.2 Dynamic-guided type

We review the two existing types of position-aware and normal SSA, as illustrated in Fig. 3(b) and (c), respectively. Then, we introduce the proposed dynamic-guided SSA.

Position-aware SSA. The position-aware attention pattern comes to one’s mind at first glance at Fig. 1(a). Based on this idea, position-aware SSA [12, 15] makes aggregation of value embeddings by a diagonal matrix \hat{A} , as shown in Fig. 3 (b). Actually, this type of static self-attention is equivalent to a convolutional layer [12]. However, it is not reasonable to assume self-attention has completely local position-aware patterns, because some global details will be ignored. We find that this type is inferior to the normal one and the proposed dynamic-guided in comparison experiments, which will be shown in Tab. 3 and 4.

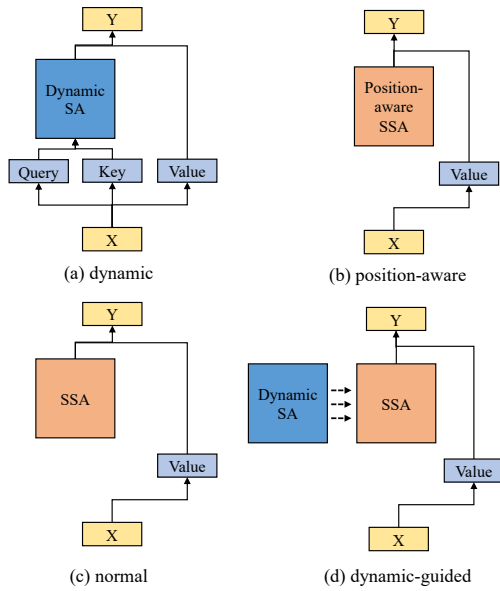


Figure 3. Dynamic self-attention (SA) and three types of static self-attention (SSA). (a) denotes dynamic SA, (b) denotes position-aware SSA used by [12, 15], (c) denotes normal SSA and (d) denotes the proposed DGSSA method, which inherits information from the dynamic SA.

Normal SSA. A full static attention matrix \hat{A} is used by normal SSA to make global aggregation of value embeddings, as shown in Fig. 3(c), thus the normal type can capture more details than the position-aware type. That explains why “normal” outperforms “local” in most settings in Tab. 3 and 4. However, normal SSA still has inferior performance to dynamic self-attention, to which we attribute that the learned attention matrix has less useful patterns due to meaningless initialization.

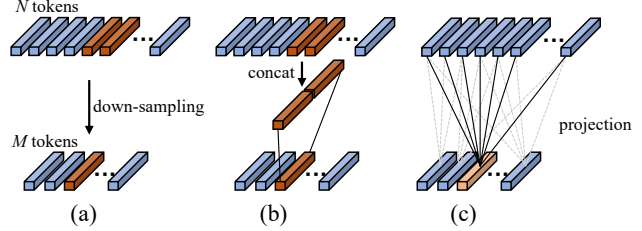


Figure 4. Different token aggregation methods of reducing N tokens to M tokens. (a) and (b) denote local down-sampling and concatenation method, respectively, while (c) denotes the proposed GLAD method, which makes global aggregation to reduce token numbers.

Dynamic-guided SSA. Considering the drawbacks of two types of static self-attention, we propose a method of dynamic-guided static self-attention. Following normal SSA, we also use a full matrix \hat{A} . Instead of training \hat{A} from scratch, we use dynamic attention matrix \hat{A} to initialize it. As shown in Fig. 3(d), the dynamic-guided SSA can inherit self-attention information from the replaced dynamic SA rather than discarding it, like normal SSA. The performance comparison of the two types validates our claim, as shown in Tab. 3 and 4.

In our opinion, the aggregated value embeddings by the static self-attention should mimic these obtained by dynamic self-attention, and thus the optimization problem is formulated to determine the optimal \hat{A} , as follows:

$$\min_{\hat{A}} \mathbb{E}_X [\|(\hat{A} - A)XW_k\|^2], \quad (3)$$

where $\|\cdot\|$ is the L_2 norm. We derive its closed-form solution as

$$\hat{A} = \mathbb{E}_X [AXW_kW_k^T X^T] (\mathbb{E}_X [XW_kW_k^T X^T])^{-1}. \quad (4)$$

Then, the optimal estimation \hat{A} can serve as meaningful initialization for the following training of the compressed ViT.

3.3. Global Aggregation Pyramid

To exploit the low-rank attention patterns in later layers, as shown in Fig. 1(b), we propose a method of global aggregation pyramid (GLAD) to reduce the token redundancy by aggregating the full number of tokens into less number. The existing local aggregation methods make down-sampling and concatenation in a fixed scope to reduce token numbers N to M , as shown in Fig. 4(a) and (b), respectively. The proposed GLAD can aggregate tokens in a global scope, as shown in Fig. 4(c).

The architecture of GLAD is shown in Fig. 2(c). Its key component consists of a linear projection $Y = WX$, where $W \in \mathbb{R}^{M \times N}$ is a trainable weight and $M < N$. The projection globally aggregates a token sequence $X \in \mathbb{R}^{N \times d}$, whose length is N , into a new sequence $Y \in \mathbb{R}^{M \times d}$, whose length is M .

LayerNorm and GeLU. Since LayerNorm and GeLU can stabilize the training and introduce additional non-linearity, respectively, we add them after the linear projection. The total formulation of GLAD is shown below:

$$Y = \text{GeLU}(\text{BatchNorm}(WX)). \quad (5)$$

Position re-embedding. The original feature sequence X is position-aware due to the added position embedding before the first layer, as [33] does. However, the linear projection of X is spatially position-free. Thus, the transformed feature Y will lose spatial information. To mitigate this problem, we add a new position embedding matrix $E \in \mathbb{R}^{M \times d}$ on Y to re-encode the position information. Thus, the Eq.5 can be re-written as:

$$Y = \text{GeLU}(\text{BatchNorm}(WX)) + E. \quad (6)$$

Token distillation. There is always a pre-trained model, denoted as vit_{pre} , in the scenario of model compression. We intend to use vit_{pre} to help the training of compressed ViTs by token distillation on the training dataset \mathcal{D} . Specifically, we use the token features X_t of vit_{pre} to distill the features Y obtained by GLAD. However, $X_t \in \mathbb{R}^{N \times d}$ and $Y \in \mathbb{R}^{M \times d}$ have different sequence length. To solve this problem, we use another instance of GLAD to transform X_t to obtain Y_t , where $Y_t \in \mathbb{R}^{M \times d}$. The grey line denotes the data flow of vit_{pre} in Fig. 2(c). The token distillation loss is defined as the MSE between features Y and Y_t , as shown below:

$$f(M; \text{vit}_{\text{pre}}, \mathcal{D}) = \|Y - Y_t\|^2. \quad (7)$$

3.4. Integrated Compression Pipeline

Based on the above two modules, we integrate DGSSA and GLAD to effectively compress a whole ViT. We insert them into a L -layer ViT which has n_l tokens in the l -th layer and has embedding dim of d , and the consecutive blocks of the compressed ViT are computed as:

$$\begin{aligned} \mathbf{x}^l &= \gamma_l \text{GLAD}(\mathbf{x}^l, m_l) + (1 - \gamma_l) \mathbf{x}^l \\ \hat{\mathbf{x}}^l &= (1 - \phi_l) \text{SA}(\text{LN}(\mathbf{x}^l)) + \phi_l \text{DGSSA}(\text{LN}(\mathbf{x}^l)) + \mathbf{x}^l \\ \mathbf{x}^{l+1} &= \text{MLP}(\text{LN}(\hat{\mathbf{x}}^l)) + \hat{\mathbf{x}}^l \end{aligned} \quad (8)$$

where binary variables γ_l and ϕ_l denotes whether DGSSA and GLAD is applied in the l -th layer, respectively. $m_l \in [1, n_l]$ is integer variable and denotes the number of left tokens in l -th layer. Variables $\gamma, \phi, \mathbf{m} \in \mathbb{R}^L$ can determine the architecture of the compressed ViT. Since their total combination possibility is too huge and there may be some unreasonable architectures, we make three constraints on them.

Constraint of γ . DGSSA is consecutively applied in the early layers (except the 0-th layer), and GLAD is excluded. For easy illustration, we introduce another scalar variable

$P \in [1, L - 1]$, which denotes that the first P layers use the SSA. Thus, there are two constraints of $\sum_{l=1}^P \gamma_l = P$ and $\sum_{l=1}^P \gamma_l * \phi_l = 0$.

Constraint of \mathbf{m} and ϕ . We also introduce a hyper-parameter Q to control the number of layers using GLAD. The constraint is formulated as $\sum_{l=P+1}^L \phi_l = Q$. And there is an implicit constraint of $m_{l_1} \geq m_{l_2}$, where $l_1 < l_2$, if $\phi_{l_1} = 1$ and $\phi_{l_2} = 1$. Thus, later layers have less left token numbers than early layers, and \mathbf{m} has a shrunk pyramid distribution across layers. That distribution is similar with pyramid structure of main-stream CNNs.

FLOPs Constraint. Another constraint is related to the compression ratio of FLOPs. The FLOPs of dynamic SA is $2n_l^2d + 4n_ld^2$, and the FLOPs of FFN is $8n_ld^2$ under the mlp ratio of 4. Thus, the total FLOPs of a ViT is $\sum_{l=0}^{L-1} 12n_ld^2 + 4n_ld^2$. The FLOPs of DGSSA is $m_l^2d + 2m_ld^2$. Thus, the total FLOPs of a compressed ViT is $\sum_{l=0}^{L-1} m_l^2d + 10m_ld^2$. We compress the original ViT under of FLOPs constraint of $\frac{\sum_{l=0}^{L-1} 10m_ld^2 + m_l^2d}{\sum_{l=0}^{L-1} 12n_ld^2 + 4n_ld^2} \leq \eta$, where η is compression ratio.

Loss formulation. The total loss \mathcal{L} comprising the task loss $\mathcal{L}_{\text{task}}$ and the GLAD loss $\mathcal{L}_{\text{glad}}$ is optimized with respect to the model weights of compressed ViT and its architecture variables under these constraints. The task loss, such as cross-entropy loss of classification tasks, is denoted as $\mathcal{L}_{\text{task}}(\mathcal{W}, \hat{A}; \gamma, \phi, \mathbf{m}, \mathcal{D})$, where \mathcal{W} and \hat{A} denotes the model weights and static self-attention matrices, respectively. The GLAD loss formulated as $\mathcal{L}_{\text{glad}} = \sum_{l=P+1}^{L-1} \phi_l \cdot f(m_l; \text{vit}_{\text{pre}}, \mathcal{D})$ based on token distillation loss taken from Eq. 7. In addition, we formulate a constrained-optimization problem to determine the optimal γ, ϕ and \mathbf{m} under hyper-parameters of P, Q and η , as follows:

$$\begin{aligned} \min_{\mathcal{W}, \hat{A}, \gamma, \phi, \mathbf{m}} \quad & \mathcal{L}(\mathcal{W}, \hat{A}, \gamma, \phi, \mathbf{m}; \text{vit}_{\text{pre}}, \mathcal{D}) \\ \text{s.t.} \quad & \sum_{l=1}^P \gamma_l = P, \sum_{l=1}^P \gamma_l * \phi_l = 0, \gamma_0 = 0 \\ & \sum_{l=P+1}^{L-1} \phi_l = Q, m_{l_1} \leq m_{l_2}, \text{ where } l_1 < l_2 \\ & \frac{\sum_{l=0}^{L-1} 10m_ld^2 + m_l^2d}{\sum_{l=0}^{L-1} 12n_ld^2 + 4n_ld^2} \leq \eta \end{aligned} \quad (9)$$

Decoupling optimization. Considering the joint optimization of \mathcal{L} with respect to weights and architecture variables is very hard, we decouple them. Firstly, γ can be determined under the constraint of γ under hyper-parameter P . Then, we design an Accuracy Metric (AM) to determine the optimal \mathbf{m} and ϕ by the constraints of \mathbf{m}, ϕ and FLOPs

under hyper-parameters Q and η , as follows:

$$\text{AM}(\mathbf{m}) = \prod_l^L \frac{\sum_i^{m_l} \sigma_{l,i}}{\sum_i^{n_l} \sigma_{l,i}}, \quad (10)$$

where $\sigma_{l,i}$ denotes the i -th expectation of singular value of self-attention matrix to the training samples at l -th layer. The optimal \mathbf{m} and ϕ are obtained by maximizing AM. We also give a dynamic programming solution in supplementary file for saving pages. Finally, we optimize the \mathcal{L} with respect to weights \mathcal{W} and \hat{A} by classical gradient descending method after determining the architecture variables.

4. Experiments

4.1. Implementation Details

Datasets. We conduct compression experiments on ILSVRC-2012 [16], which has 1.28M colored training images and 50K colored validation images from 1K classes. The top-1 accuracy on a single crop is reported.

Training settings. The training settings mainly follow Deit [33] and Swin [23]. We use an AdamW [21] optimizer with a learning rate initialized as 0.001 and decayed by $1e^{-5}$ with the cosine strategy. The weight decay of 0.05 is adopted. The training lasts for 300 epochs with a linear warm-up used in the first 5 epochs, and the learning rate of warm-up is $1e^{-6}$. We also use the same data augmentation and regularization settings as Deit. All models are trained on NVIDIA V100 8 GPUs with a batch size of 1024 for DGSSA-based compression and a batch size of 4096 for the GLAD-based and integrated pipeline compression. Following [28], we adopt self-supervised distill training. Specifically, we optimize cross-entropy loss to minimize the difference between predictions of a original pre-trained ViT and the compressed one.

Compression configurations. 1) Configurations of Deit. To achieve around 100% increased throughput, compression ratio η of Deit-Small and Deit-Base is set to be around 0.5. The η of Deit-Tiny is 0.54, since Deit-Tiny is more compact. The hyper-parameter P is 2 based on the empirical experiment results in Tab. 3. Too large Q will introduce much additional overhead computation of GLAD, while too small Q will lead to bad compression results. Thus, we empirically set hyper-parameter Q as 3. 2) Configurations of Swin. The compression ratio η is set to be 0.1, since Swin already has been quite efficient. The hyper-parameter P is set to be 6, 12 and 12 in the compression configurations of Swin-Tiny, Swin-Small and Swin-Base, respectively. Above all, γ_l is determined under P , while ϕ_l and m_l can be determined by maximizing AM in Eq.10 under Q and η . All configurations can be found in Tab. 2.

Taking Our-Deit-S in Tab. 2 as an example to interpret the configuration. DGSSA is applied at the 1-th and 2-nd

layer. The token numbers 197 is reduced to 127, 77 and 35 when GLAD is applied at 3-th, 5-th and 7-th layer.

4.2. Results on ILSVRC-2012

In this section, we compress two typical ViTs of Deit [33] and Swin [23] on ILSVRC-2012. We use the integrated pipeline of DGSSA and GLAD to compress Deit-Tiny, Small and Base, and the results are denoted as Integrated-Deit-T, S and B. We only use DGSSA to compress the early layers of Swin-Tiny, Small and Base, since Swin has already a pyramid distribution of token numbers. The results are denoted as DGSSA-Swin-T, S and B. The configurations of compression are shown in Tab. 2.

As shown in Tab. 1, our integrated compression pipeline can increase the run-time throughput of Deit-Tiny, Small and Base by 73.9%, 121.1% and 113.0%, respectively. The increased throughput is much higher than previous state-of-the-art methods of Evo [40], PS [31], DynamicViT [28] and TOME [3] by a large margin. It is notable that Integrated-Deit-S has no accuracy drop despite making so much acceleration. Meanwhile, Integrated-Deit-T and B can accelerate Deit-Small and Base much more than these methods with 0.1 % and 0.3% accuracy drop. The comparison verifies the effectiveness of the proposed integrated pipeline. Moreover, new state-of-the-art compression results of Deit are produced.

Even though Swin has already been quite efficient, DGSSA-based compression can increase the throughput of the baselines by 9.0%, 10.5% and 10.0% with 0.0%, 0.0% and 0.1% accuracy drop, respectively. The successful compression results can verify that the DGSSA can be applied to not only the global self-attention used by Deit but also the local window attention used by Swin.

4.3. Ablation Studies on DGSSA

Limited scalability of SSA. We make experiments to explore the scalability of DGSSA. In the experiments, DGSSA is applied to the first 2, 4, 6, 8, 10 layers of Deit-S and the first 6, 12, 18 and 20 layers of Swin-S, respectively.

There is no accuracy drop after DGSSA is applied in the first 2 layers of Deit-Small and in the first 6 layers of Swin-Small, as shown in Tab. 3 and Tab. 4, respectively. When the number of static layers increases, the accuracy of “DG” decreases. When 10 layers out of total 12 layers apply DGSSA on Deit, the accuracy severely drops from 79.9% to 78.18% by 1.72%, which is unbearable accuracy gap. The results suggest that *SSA can only be applied in the few first layers*. The conclusion accords with the difference metric in Fig. 5, which shows that the early layers have relatively small difference metric value in general. According to the conclusion, MLP-Mixer is unreasonable because it assumes that all layers are static.

Dynamic-guided way v.s. others. We investigate the

Table 1. Comparison of compressed ViTs with previous methods on ILSVRC-2012. Following [23, 33], we measure throughput based on the public code on a V100 GPU. * means that 428.8 is our measured speed while 436.9 is the value provide by [23].

Model	Method	Param	FLOPs	Throughput		Top-1 Acc. (%)
				(img/s)	↑(%)	
Deit	Deit-Tiny [33] (baseline)	5.7M	1.3G	2536	-	72.2
	S ² ViTE [7]	4.2M	1.0G	-	11.8	70.1
	Evo-Deit-T [40]	-	-	4027	58.8	72.0
	PS-Deit-T [31]	-	0.7G	-	68.1	72.0
	TPS [37]	5.9M	0.8G	-	-	72.9
	Integrated-Deit-T(ours)	5.7M	0.7G	4410	73.9	72.1
	Deit-Small [33] (baseline)	22.1M	4.6G	940	-	79.9
	S ² ViTE [7]	14.6M	3.1G	-	29.3	79.2
	IA-RED ² [24]	-	-	-	46.2	79.1
	Evo-Deit-S [40]	-	-	1510	60.6	79.4
	PS-Deit-S [31]	-	2.6G	-	64.5	79.4
	DynamicViT-Deit-S [28]	-	4.0G	1525	62.2	79.8
	ATS [18]	22.1M	2.9G	-	-	79.7
	TPS [37]	22.1M	3.0G	-	-	80.1
	TOME [3]	-	2.7G	1550	64.9	79.4
	GLAD-Deit-S(ours)	22.2M	2.3G	1934	106.0	79.9
	Integrated-Deit-S(ours)	21.6M	2.1G	2080	121.1	79.9
	Deit-Base [33](baseline)	86.6M	17.5G	292	-	81.8
	IA-RED ² [24]	-	-	-	37.5	80.9
	Evo-Deit-B [40]	-	-	462	54.5	81.3
PS-Deit-B [31]	-	9.8G	-	67.8	81.5	
Integrated-Deit-B(ours)	84.5M	8.6G	622	113.0	81.6	
Swin	Swin-T [23](baseline)	29.0M	4.5G	755.2	-	81.3
	DGSSA-Swin-T(ours)	28.5M	4.1G	823	9.0	81.3
	Swin-S [23](baseline)	49.6M	8.7G	428.8(436.9)*	-	83.0
	DGSSA-Swin-S(ours)	48.7M	8.0G	474	10.5	83.0
	Swin-B [23](baseline)	87.8M	15.4G	278.1	-	83.5
	DGSSA-Swin-B(ours)	85.4M	14.1G	306	10.0	83.4

Table 2. Configurations of our compressed ViTs in Tab. 1

	SSA		GLAD	
	P	Q	ϕ	m
Integrated-Deit-T	2	3	ϕ_3, ϕ_5, ϕ_7	197 → 152 → 107 → 62
Integrated-Deit-S	2	3	ϕ_3, ϕ_5, ϕ_7	197 → 127 → 77 → 35
Integrated-Deit-B	2	3	ϕ_3, ϕ_5, ϕ_7	197 → 143 → 89 → 35
DGSSA-Swin-T	6	-	-	-
DGSSA-Swin-S	12	-	-	-
DGSSA-Swin-B	12	-	-	-

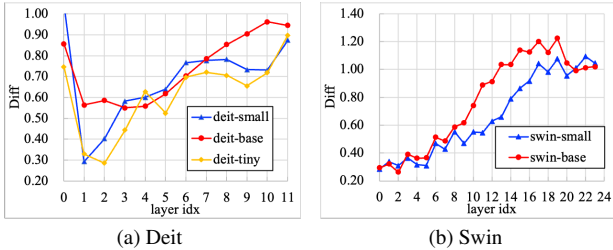


Figure 5. The metric measuring the difference between estimated static self-attention and dynamic self-attention across layers in Deit and Swin. The early layers, except 0-th layer in Deit, have smaller difference metric value than later layers in general.

effectiveness of the proposed DGSSA, denoted as “DG”, by making comparison experiments with normal, local position-aware self-attention [12, 15] and MLP-Mixer [32] under the comparable calculation complexity. “nomral” trains the static self-attention matrix from random initialization. Works like [12, 15], denoted as “local”, use a position-

Table 3. Dynamic-guided way outperforms other two types of static self-attention and MLPs on Deit-Small. “F2Ls” denotes the results when static self-attention or MLPs is applied in the first 2 layers (F2Ls) of Deit-Small. DG refers to the proposed DGSSA. We train all models for 100 epochs for saving computation.

	Types	F2Ls	F4Ls	F6Ls	F8Ls	F10Ls
Deit-S	DG	79.99	79.73	79.34	78.87	78.18
	normal	79.96	79.55	78.99	78.59	77.90
	local [12]	79.94	79.48	78.73	77.98	77.08
	MLPs [32]	79.36	77.90	75.80	73.84	73.19

Table 4. Dynamic-guided way outperforms other two types of static self-attention and MLPs on Swin-Small. Refer to Tab. 3 for the meaning of denotations. We train all models for 50 epochs for saving computation.

	Types	F6Ls	F12Ls	F18Ls	F20Ls
Swin-S	DG	83.00	82.63	81.68	81.39
	normal	82.82	82.36	81.54	81.15
	local [12]	82.66	81.93	80.33	79.96
	MLPs [32]	82.10	80.64	77.26	76.51

aware static self-attention matrix and their implementation follows the public code ¹. MLP-Mixer, denoted as “MLPs”, is also a static network. We make its implementation from the code ², and the token dimension is kept default value

¹<https://github.com/facebookresearch/convit>

²<https://github.com/rishikksh20/MLP-Mixer-pytorch>

while the channel dimension is adjusted to ensure the comparable calculation complexity.

The results are shown in Tab. 3 and 4, from which we can notice that the proposed “DG” outperforms “random”, “MLPs” and “local” under different configurations of self-attention and on two kinds of ViTs of Deit-S and Swin-S. The useful information inherited from the replaced dynamic self-attention can serve as good initialization in the dynamic-guided way. By contrast, “normal” trains their self-attention matrices from scratch. Thus, the *good initialization* may account for its effectiveness.

Moreover, both global “DG” and “normal” outperform “local” in Tab. 3 and 4, which may result from that the local position-aware patterns may lose some global details due to the limited receptive field. Since the position-aware self-attention is equivalent to CNNs with kernel size of square root of head number, the conclusion may indicate that CNNs may not be a good choice to relieve the computation of early layers for ViTs.

Finally, MLP-Mixer has the worst performance in all configurations. Then, we can make conclusion that making self-attention module of ViTs static is better than mixing MLP-Mixer blocks into ViTs in early layers.

4.4. Ablation Studies on GLAD

In this part, we compare GLAD with other pruning-based and aggregation-based methods to illustrate the effectiveness of GLAD.

Comparison with pruning-based methods. As shown in Tab. 1, GLAD-based compression outperforms other pruning-based methods, such as Evo [40], PS [31], DynamicViT [28] and TOME [3] in terms of throughput and accuracy on Deit-Small. The reasons may come from two folds: 1) pruning-based methods will lose spatial information after reducing token numbers, while GLAD can preserve the information as much as possible while reducing token spatial size by a linear aggregation. 2) GLAD is more efficient in run-time mode due to no need of importance score prediction module which is adopted by DynamicViT [28] during inference.

Comparison with aggregation-based methods. We also make controlled comparison experiments to compare GLAD with other aggregation-based methods, such as the local concatenation used in Swin [23] and Twins [10], and down-sampling used in [38]. To make fair comparison, we control the same aggregated token numbers and do not use DGSSA method in the early layers in all experiments.

As shown in Tab. 5, GLAD outperforms concatenation and down-sampling methods. Global GLAD has improvement of 0.4 % and 0.3 % Top-1 accuracy over local concatenation and down-sampling methods, respectively. The feature of “global” may account for the performance. The two local methods aggregate tokens to get less token numbers

Table 5. The comparison of GLAD with other aggregation-based methods of reducing token numbers.

Methods	Scope	Top-1 Acc.(%)
GLAD	global	80.4
concatenation [10, 23]	local	80.0
down-sampling [38]	local	80.1

within a fixed-size window, such as 2×2 . The pre-defined fixed size may not be suitable for the real distribution of feature redundancy information. Above all, the comparison results validate the *effectiveness of GLAD which makes global aggregation*.

4.5. Integrated pipeline v.s. single usage

In this section, we make comparison experiments to illustrate that the integrated usage of DGSSA and GLAD is better than single usage. We use Integrated-Deit-S as the baseline. Integrated-Deit-S uses DGSSA in the first two layers and applies GLAD in the later layers (3-th, 5-th and 7-th layer). A1 and A2 are counterparts of Integrated-Deit-S under comparable throughput. Specifically, A1 drops GLAD and still uses DGSSA in the later layers, while A2 drops the DGSSA and still uses GLAD in the first two layers on the base of Integrated-Deit-S. The configurations of B1 and B2 adopt the subset of the configuration used by Integrated-Deit-S. Specifically, B1 drops GLAD in the later layers, while B2 drops the DGSSA in the first two layers on the base of Integrated-Deit-S.

We can make two conclusions from the results shown in Tab. 6. Firstly, GLAD-based compression of A2 causes 0.5% accuracy drop under comparable acceleration, while DGSSA-based compression of A1 cannot produce so much acceleration. Thus, *the integrated compression is much more effective than single usage under comparable throughput*. Secondly, integrated-Deit-S further uses DGSSA in the first two layers on the base of B2 and yields +146 img/s without accuracy drop. Compared with B1, Integrated-Deit-S further uses GLAD in the later layers and obtain +1057 img/s without accuracy drop too. The comparison illustrates that *integrated usage can make further acceleration on the base of single usage without accuracy drop*.

Table 6. Results of ablation study of integrated pipeline. Integrated-Deit-S is the baseline. “all” means the counterpart configurations, in which DGSSA or GLAD is applied in both early and later layers, under comparable throughput. “partial” means configurations which are subset of configurations used by Integrated-Deit-S. Following [23, 33], we measure throughput on a V100 GPU.

No.	Configuration	Throughput (img/s)	Top-1 Acc. (%)
Integrated-Deit-S	DGSSA+GLAD	2080	79.9
A1	all DGSSA	1200	78.2
A2	all GLAD	2108	79.4
B1	partial DGSSA	1023	79.9
B2	partial GLAD	1934	79.9

5. Conclusion

In this paper, we observe that ViTs have heterogeneous self-attention patterns that attention maps have more similar patterns across different images in early layers than later layers, while have more low-rank patterns in later layers than early layers. Inspired by the observations, we propose an integrated compression pipeline of dynamic-guided static self-attention (DGSSA) and global aggregation pyramid (GLAD) to accelerate the whole ViTs. The advantages of DGSSA and GLAD over previous methods are verified by extensive ablation studies, respectively. Moreover, the integrated pipeline produces new SOTA results that Deit can be accelerated by up to 121% with negligible accuracy drop. In the future, we will determine the hyper-parameters P and Q for the better use of the integrated pipeline by automatic machine learning techniques and other strategies.

References

- [1] Joshua Ainslie, Santiago Ontanon, Chris Alberti, Vaclav Cvicek, Zachary Fisher, Philip Pham, Anirudh Ravula, Sumit Sanghai, Qifan Wang, and Li Yang. Etc: Encoding long and structured inputs in transformers. *arXiv preprint arXiv:2004.08483*, 2020. 1, 2
- [2] Iz Beltagy, Matthew E Peters, and Arman Cohan. Longformer: The long-document transformer. *arXiv preprint arXiv:2004.05150*, 2020. 1, 2
- [3] Daniel Bolya, Cheng-Yang Fu, Xiaoliang Dai, Peizhao Zhang, Christoph Feichtenhofer, and Judy Hoffman. Token merging: Your vit but faster. *arXiv preprint arXiv:2210.09461*, 2022. 3, 6, 7, 8
- [4] Nicolas Carion, Francisco Massa, Gabriel Synnaeve, Nicolas Usunier, Alexander Kirillov, and Sergey Zagoruyko. End-to-end object detection with transformers. In *European Conference on Computer Vision*, pages 213–229. Springer, 2020. 1
- [5] Nicolas Carion, Francisco Massa, Gabriel Synnaeve, Nicolas Usunier, Alexander Kirillov, and Sergey Zagoruyko. End-to-end object detection with transformers. In *European Conference on Computer Vision*, pages 213–229, 2020. 1
- [6] Hanting Chen, Yunhe Wang, Tianyu Guo, Chang Xu, Yiping Deng, Zhenhua Liu, Siwei Ma, Chunjing Xu, Chao Xu, and Wen Gao. Pre-trained image processing transformer. In *Proceedings of the IEEE/CVF Conference on Computer Vision and Pattern Recognition*, pages 12299–12310, 2021. 1
- [7] Tianlong Chen, Yu Cheng, Zhe Gan, Lu Yuan, Lei Zhang, and Zhangyang Wang. Chasing sparsity in vision transformers: An end-to-end exploration. *arXiv preprint arXiv:2106.04533*, 2021. 7
- [8] Rewon Child, Scott Gray, Alec Radford, and Ilya Sutskever. Generating long sequences with sparse transformers. *arXiv preprint arXiv:1904.10509*, 2019. 1
- [9] Rewon Child, Scott Gray, Alec Radford, and Ilya Sutskever. Generating long sequences with sparse transformers. *arXiv preprint arXiv:1904.10509*, 2019. 2
- [10] Xiangxiang Chu, Zhi Tian, Yuqing Wang, Bo Zhang, Haibing Ren, Xiaolin Wei, Huaxia Xia, and Chunhua Shen. Twins: Revisiting the design of spatial attention in vision transformers. *arXiv preprint arXiv:2104.13840*, 1(2):3, 2021. 1, 3, 8
- [11] Xiangxiang Chu, Zhi Tian, Bo Zhang, Xinlong Wang, Xiaolin Wei, Huaxia Xia, and Chunhua Shen. Conditional positional encodings for vision transformers. *arXiv preprint arXiv:2102.10882*, 2021. 1
- [12] Jean-Baptiste Cordonnier, Andreas Loukas, and Martin Jaggi. On the relationship between self-attention and convolutional layers. *arXiv preprint arXiv:1911.03584*, 2019. 4, 7
- [13] Xiyang Dai, Yinpeng Chen, Jianwei Yang, Pengchuan Zhang, Lu Yuan, and Lei Zhang. Dynamic detr: End-to-end object detection with dynamic attention. In *Proceedings of the IEEE/CVF International Conference on Computer Vision*, pages 2988–2997, 2021. 1
- [14] Zhigang Dai, Bolun Cai, Yugeng Lin, and Junying Chen. Up-detr: Unsupervised pre-training for object detection with transformers. In *Proceedings of the IEEE/CVF Conference on Computer Vision and Pattern Recognition*, pages 1601–1610, 2021. 1
- [15] Stéphane d’Ascoli, Hugo Touvron, Matthew Leavitt, Ari Morcos, Giulio Biroli, and Levent Sagun. Convit: Improving vision transformers with soft convolutional inductive biases. *arXiv preprint arXiv:2103.10697*, 2021. 2, 4, 7
- [16] Jia Deng, Wei Dong, Richard Socher, Li-Jia Li, Kai Li, and Li Fei-Fei. Imagenet: A large-scale hierarchical image database. In *Proceedings of the IEEE/CVF Conference on Computer Vision and Pattern Recognition*, pages 248–255. Ieee, 2009. 1, 6
- [17] Alexey Dosovitskiy, Lucas Beyer, Alexander Kolesnikov, Dirk Weissenborn, Xiaohua Zhai, Thomas Unterthiner, Mostafa Dehghani, Matthias Minderer, Georg Heigold, Sylvain Gelly, et al. An image is worth 16×16 words: Transformers for image recognition at scale. *arXiv preprint arXiv:2010.11929*, 2020. 1
- [18] Mohsen Fayyaz, Soroush Abbasi Koohpayegani, Farnoush Rezaei Jafari, Sunando Sengupta, Hamid Reza Vaezi Joze, Eric Sommerlade, Hamed Pirsiavash, and Jürgen Gall. Adaptive token sampling for efficient vision transformers. In *Computer Vision—ECCV 2022: 17th European Conference, Tel Aviv, Israel, October 23–27, 2022, Proceedings, Part XI*, pages 396–414. Springer, 2022. 3, 7
- [19] Kai Han, An Xiao, Enhua Wu, Jianyuan Guo, Chunjing Xu, and Yunhe Wang. Transformer in transformer. *arXiv preprint arXiv:2103.00112*, 2021. 1
- [20] Zihang Jiang, Qibin Hou, Li Yuan, Daquan Zhou, Xiaojie Jin, Anran Wang, and Jiashi Feng. Token labeling: Training a 85.5% top-1 accuracy vision transformer with 56m parameters on imagenet. *arXiv preprint arXiv:2104.10858*, 2021. 1
- [21] Diederik P Kingma and Jimmy Ba. Adam: A method for stochastic optimization. *arXiv preprint arXiv:1412.6980*, 2014. 6

- [22] Nikita Kitaev, Łukasz Kaiser, and Anselm Levskaya. Reformer: The efficient transformer. *arXiv preprint arXiv:2001.04451*, 2020. 1, 2
- [23] Ze Liu, Yutong Lin, Yue Cao, Han Hu, Yixuan Wei, Zheng Zhang, Stephen Lin, and Baining Guo. Swin transformer: Hierarchical vision transformer using shifted windows. *arXiv preprint arXiv:2103.14030*, 2021. 1, 3, 6, 7, 8
- [24] Bowen Pan, Rameswar Panda, Yifan Jiang, Zhangyang Wang, Rogerio Feris, and Aude Oliva. Ia-red²: Interpretability-aware redundancy reduction for vision transformers. *arXiv preprint arXiv:2106.12620*, 2021. 7
- [25] Niki Parmar, Ashish Vaswani, Jakob Uszkoreit, Łukasz Kaiser, Noam Shazeer, Alexander Ku, and Dustin Tran. Image transformer. In *International Conference on Machine Learning*, pages 4055–4064. PMLR, 2018. 1, 2
- [26] Jiezhong Qiu, Hao Ma, Omer Levy, Scott Wen-tau Yih, Sinong Wang, and Jie Tang. Blockwise self-attention for long document understanding. *arXiv preprint arXiv:1911.02972*, 2019. 1, 2
- [27] Alessandro Raganato, Yves Scherrer, and Jörg Tiedemann. Fixed encoder self-attention patterns in transformer-based machine translation. *arXiv preprint arXiv:2002.10260*, 2020. 1, 2
- [28] Yongming Rao, Wenliang Zhao, Benlin Liu, Jiwen Lu, Jie Zhou, and Cho-Jui Hsieh. Dynamicvit: Efficient vision transformers with dynamic token sparsification. *arXiv preprint arXiv:2106.02034*, 2021. 1, 3, 6, 7, 8
- [29] Aurko Roy, Mohammad Saffar, Ashish Vaswani, and David Grangier. Efficient content-based sparse attention with routing transformers. *Transactions of the Association for Computational Linguistics*, 9:53–68, 2021. 2
- [30] Aravind Srinivas, Tsung-Yi Lin, Niki Parmar, Jonathon Shlens, Pieter Abbeel, and Ashish Vaswani. Bottleneck transformers for visual recognition. In *Proceedings of the IEEE/CVF Conference on Computer Vision and Pattern Recognition*, pages 16519–16529, 2021. 1
- [31] Yehui Tang, Kai Han, Yunhe Wang, Chang Xu, Jianyuan Guo, Chao Xu, and Dacheng Tao. Patch slimming for efficient vision transformers. *arXiv preprint arXiv:2106.02852*, 2021. 1, 3, 6, 7, 8
- [32] Ilya Tolstikhin, Neil Houlsby, Alexander Kolesnikov, Lucas Beyer, Xiaohua Zhai, Thomas Unterthiner, Jessica Yung, Daniel Keysers, Jakob Uszkoreit, Mario Lucic, et al. Mlp-mixer: An all-mlp architecture for vision. *arXiv preprint arXiv:2105.01601*, 2021. 1, 2, 7
- [33] Hugo Touvron, Matthieu Cord, Matthijs Douze, Francisco Massa, Alexandre Sablayrolles, and Hervé Jégou. Training data-efficient image transformers & distillation through attention. In *International Conference on Machine Learning*, pages 10347–10357. PMLR, 2021. 1, 5, 6, 7, 8
- [34] Sinong Wang, Belinda Z Li, Madian Khabsa, Han Fang, and Hao Ma. Linformer: Self-attention with linear complexity. *arXiv preprint arXiv:2006.04768*, 2020. 2
- [35] Wenhai Wang, Enze Xie, Xiang Li, Deng-Ping Fan, Kaitao Song, Ding Liang, Tong Lu, Ping Luo, and Ling Shao. Pyramid vision transformer: A versatile backbone for dense prediction without convolutions. *arXiv preprint arXiv:2102.12122*, 2021. 1
- [36] Yuqing Wang, Zhaoliang Xu, Xinlong Wang, Chunhua Shen, Baoshan Cheng, Hao Shen, and Huaxia Xia. End-to-end video instance segmentation with transformers. In *Proceedings of the IEEE/CVF Conference on Computer Vision and Pattern Recognition*, pages 8741–8750, 2021. 1
- [37] Siyuan Wei, Tianzhu Ye, Shen Zhang, Yao Tang, and Jiajun Liang. Joint token pruning and squeezing towards more aggressive compression of vision transformers. In *Proceedings of the IEEE/CVF Conference on Computer Vision and Pattern Recognition*, pages 2092–2101, 2023. 3, 7
- [38] Haiping Wu, Bin Xiao, Noel Codella, Mengchen Liu, Xiyang Dai, Lu Yuan, and Lei Zhang. Cvt: Introducing convolutions to vision transformers. *arXiv preprint arXiv:2103.15808*, 2021. 1, 3, 8
- [39] Enze Xie, Wenhai Wang, Zhiding Yu, Anima Anandkumar, Jose M Alvarez, and Ping Luo. Segformer: Simple and efficient design for semantic segmentation with transformers. *arXiv preprint arXiv:2105.15203*, 2021. 1
- [40] Yifan Xu, Zhijie Zhang, Mengdan Zhang, Kekai Sheng, Ke Li, Weiming Dong, Liqing Zhang, Changsheng Xu, and Xing Sun. Evo-vit: Slow-fast token evolution for dynamic vision transformer. *arXiv preprint arXiv:2108.01390*, 2021. 1, 3, 6, 7, 8
- [41] Li Yuan, Yunpeng Chen, Tao Wang, Weihao Yu, Yujun Shi, Zihang Jiang, Francis EH Tay, Jiashi Feng, and Shucheng Yan. Tokens-to-token vit: Training vision transformers from scratch on imagenet. *arXiv preprint arXiv:2101.11986*, 2021. 1
- [42] Yuhui Yuan, Rao Fu, Lang Huang, Weihong Lin, Chao Zhang, Xilin Chen, and Jingdong Wang. Hrformer: High-resolution transformer for dense prediction. In *Advances in Neural Information Processing Systems*, 2021. 1
- [43] Manzil Zaheer, Guru Guruganesh, Kumar Avinava Dubey, Joshua Ainslie, Chris Alberti, Santiago Ontanon, Philip Pham, Anirudh Ravula, Qifan Wang, Li Yang, et al. Big bird: Transformers for longer sequences. In *Advances in Neural Information Processing Systems*, 2020. 1, 2
- [44] Sixiao Zheng, Jiachen Lu, Hengshuang Zhao, Xiatian Zhu, Zekun Luo, Yabiao Wang, Yanwei Fu, Jianfeng Feng, Tao Xiang, Philip HS Torr, et al. Rethinking semantic segmentation from a sequence-to-sequence perspective with transformers. In *Proceedings of the IEEE/CVF Conference on Computer Vision and Pattern Recognition*, pages 6881–6890, 2021. 1
- [45] Chen Zhu, Wei Ping, Chaowei Xiao, Mohammad Shoeybi, Tom Goldstein, Anima Anandkumar, and Bryan Catanzaro. Long-short transformer: Efficient transformers for language and vision. *arXiv preprint arXiv:2107.02192*, 2021. 2
- [46] Xizhou Zhu, Weijie Su, Lewei Lu, Bin Li, Xiaogang Wang, and Jifeng Dai. Deformable detr: Deformable transformers for end-to-end object detection. *arXiv preprint arXiv:2010.04159*, 2020. 1